Two-dimensional collision of probe photons with relativistic ionization fronts

J. M. Dias,[1,*] N. C. Lopes,[1] L. O. Silva,[1,2] G. Figueira,[1] and J. T. Mendonça[1]
[1]*GoLP/Centro de Física de Plasmas, Instituto Superior Técnico, 1049-001 Lisboa, Portugal*
[2]*Department of Physics and Astronomy, University of California Los Angeles, Los Angeles, California 90095*
(Received 30 March 2001; published 13 February 2002)

The collision of a probe laser pulse with a relativistic ionization front is analyzed via two-dimensional ray-tracing theory and simulations. It is shown that collisions in higher dimensions lead to new regimes for the frequency upshift of the probe photons; the frequency upshift can be considerably higher for particular collision angles that maximize the interaction length with the ionization front gradient. Finite ionization fronts also lead to angle-dependent frequency upshifts, thus acting as diffraction gratings.

DOI: 10.1103/PhysRevE.65.036404 PACS number(s): 52.38.−r, 42.15.Dp

The frequency upshift of electromagnetic waves interacting with relativistic ionization fronts or relativistic electron plasma waves has been raising significant interest in connection with tunable radiation sources [1–8], diagnostics for plasma-based accelerators [9], and ionization dynamics experiments [10,11]; the collision of weak electromagnetic fields with relativistically moving plasma perturbations can lead to significant frequency upshifts which can be controlled and can give information about the structure of the ionization front or laser wakefield.

Despite the detailed study performed by Lampe, Ott, and Walker in their seminal paper [2], where the collision of an oblique wave incidence with an infinite ionization front was first considered, most of the theoretical work has been focused on one-dimensional configurations, even though, in general, experiments are intrinsically two-dimensional or contain higher-dimensional features, such as ionization front finite width or probe beams with finite transverse profiles. Motivated by recent experimental work with two-dimensional collisions of relativistic ionization fronts and weak short laser pulses [12], we investigate the key features of the frequency upshift of the probe pulse, combining theoretical results for two-dimensional infinite fronts with ray-tracing simulations. In particular, we identify the different qualitative regimes for frequency upshift and we explore the effects arising from finite ionization fronts: it is shown that finite ionization fronts (with widths comparable to the interaction length of the probe photons with the front) lead to lower upshifts, and more important, this upshift is less sensitive to the front velocity, and essentially dependent on the maximum electron density of the ionization front for all collision angles. Furthermore, we demonstrate that under appropriate conditions it is possible to employ a finite ionization front simultaneously for frequency upshift and pulse chirping: finite ionization fronts thus act as diffraction gratings that increase the available laser bandwidth. The analytic results are complemented by ray-tracing simulations of the probe photons, obtained by numerically solving the ray-tracing equations.

We start with the ray-tracing equations, written in Hamiltonian form, and valid in the limit of the geometrical optics approximation, which means that the ionization front longitudinal dimension ($\tau_f c$, where τ_f is the ionization front rise time) and the transverse dimension ($2W_0$) are much larger than the probe photons wavelength [13]:

$$\dot{\mathbf{k}} = \frac{d\mathbf{k}}{dt} = -\frac{\partial \Omega}{\partial \mathbf{x}} = -\frac{1}{2\Omega}\frac{\partial \omega_{pe}^2}{\partial \mathbf{x}}, \tag{1}$$

$$\dot{\mathbf{x}} = \frac{d\mathbf{x}}{dt} = \frac{\partial \Omega}{\partial \mathbf{k}} = \frac{\mathbf{k}c^2}{\Omega}, \tag{2}$$

$$\dot{\Omega} = \frac{d\Omega}{dt} = \frac{\partial \Omega}{\partial t} = \frac{1}{2\Omega}\frac{\partial \omega_{pe}^2}{\partial t}, \tag{3}$$

where $\Omega = [\mathbf{k}^2 c^2 + \omega_{pe}^2(\mathbf{x},t)]^{1/2}$, the local frequency, as determined from the linear dispersion relations, plays the role of the Hamiltonian, and $\mathbf{k}$ and $\mathbf{x}$ are the canonical momentum, or wave vector, and canonical position, respectively, and $\omega_p^2(\mathbf{x},t) = 4\pi e^2 n_e(\mathbf{x},t)/m_e$ is the local electron plasma frequency squared, where $n_e(\mathbf{x},t)$ is the local electron density of the ionization front, m_e is the electron mass, and e is the electron charge. We will assume that the short laser pulse, characterized by $\mathbf{k}$, $\mathbf{x}$, and Ω, propagates in the presence of an ionization front described by the electron density perturbation

$$\omega_{pe}^2(x - \beta_f c t) = \omega_{pe0}^2\{1 - \Theta(x - \beta_f c t)\}, \tag{4}$$

where x is the ionization front propagation direction, $\beta_f c \mathbf{e}_x$ the ionization front velocity, and Θ the Heaviside function such that $\Theta(x) = 1$ for $x < 0$, and $\Theta(x) = 0$ otherwise. We stress, however, that for an infinite front the exact shape of the ionization front does not change our results. It is possible to assume that the ionization front is infinite whenever two conditions are met: (i) the transverse width of the front is larger than the probe beam width, (ii) the transverse propagation length of the probe photons is shorter than the ionization front width, i.e., $\tau_f c \sin\theta_0/(\beta_f - \cos\theta_0) \ll 2W_0$. We will assume that $\mathbf{k}$ is defined in the xy plane, and $\cos\theta_0 = \mathbf{k}\cdot\mathbf{e}_x/|\mathbf{k}|$. With this definition, the standard results for the frequency upshift in co- and counterpropagation will be recovered for $\theta_0 = 0$, and $\theta_0 = \pi$, respectively. We follow the

*Electronic address: jmdias@alfa.ist.utl.pt

procedure described elsewhere [8], introducing the canonical transformation defined by the generating function

$$F_2 = p_x(x - \beta_f ct) + p_y y, \tag{5}$$

corresponding to the change of variables

$$p_x = k_x, \quad p_y = k_y, \tag{6}$$

$$\eta_x = x - \beta_f ct, \quad \eta_y = y, \tag{7}$$

and the new Hamiltonian $\overline{\Omega}$ satisfies

$$\overline{\Omega} = [(p_x^2 + p_y^2)c^2 + \omega_{pe}^2(\eta_x)]^{1/2} - p_x \beta_f c, \tag{8}$$

and it is independent of η_y, which means that $p_y = k_y$ is a constant of the motion. Furthermore, since now $\overline{\Omega}$ is also independent of t, then $\overline{\Omega}$ is another constant of the motion. We will use these two constants of motion to derive the frequency upshift for different configurations.

We first consider that the probe photons propagate in vacuum which means that $\omega_0 = k_0 c$, with $k_0 = (p_{x0}^2 + p_{y0}^2)^{1/2}$, and $p_{x0} = k_0 \cos\theta_0$, and $p_{y0} = k_0 \sin\theta_0$. With these initial conditions $\overline{\Omega}(t=0) = \omega_0(1 - \beta_f \cos\theta_0)$. After collision with the ionization front, the photons can be either reflected by the front (and propagate in vacuum), or transmitted across the front (and propagate in the plasma region). The first scenario occurs whenever the trajectory $p_x(\eta_x, \eta_y)$ has a caustic, i.e., $\partial p_x / \partial \eta_x = -\infty$, which leads to the condition $\omega_0 \leqslant \omega_\eta$, where ω_η is defined by

$$\omega_\eta^2 = \frac{\omega_{pe0}^2(1 - \beta_f^2)}{(1 - \beta_f \cos\theta_0)^2 - (1 - \beta_f^2)\sin^2\theta_0}. \tag{9}$$

If $\omega_0 \leqslant \omega_\eta$ the pulse is reflected by the front and the maximum frequency ω_f of the photon after the collision is given by

$$\frac{\omega_f}{\omega_0} = \frac{1 - \beta_f \cos\theta_0}{1 - \beta_f^2} + \frac{|\beta_f|}{1 - \beta_f^2}|\beta_f - \cos\theta_0|. \tag{10}$$

This regime describes not only the standard double relativistic Doppler upshift in counterpropagation ($\theta_0 = \pi$), but it also describes the scenario where the photons are overtaken by the front and reflected to the vacuum region.

On the other hand, when $\omega_0 > \omega_\eta$ the photons will propagate in the plasma region (behind the front) and the maximum frequency ω_f is

$$\frac{\omega_f}{\omega_0} = \frac{1 - \beta_f \cos\theta_0}{1 - \beta_f^2} - \frac{|\beta_f|}{1 - \beta_f^2}\left[(\beta_f - \cos\theta_0)^2 - \frac{\omega_{pe0}^2}{\omega_0^2}(1 - \beta_f^2)\right]^{1/2}. \tag{11}$$

In this scenario an additional regime can be identified, when the probe photons are reflected (i.e., p_x changes sign) but the photons propagate behind the front. The maximum cutoff frequency ω_X for this regime can be obtained from the condition $p_x = 0$ for some point in the photon trajectory:

$$\omega_X^2 = \frac{\omega_{pe0}^2}{(1 - \beta_f \cos\theta_0)^2 - \sin^2\theta_0} > 0. \tag{12}$$

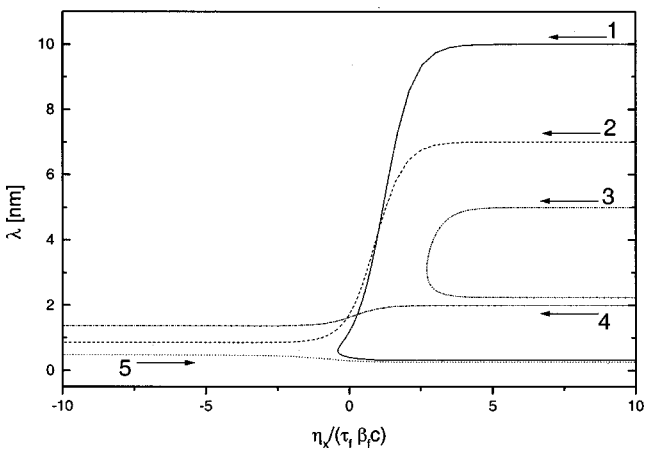

FIG. 1. Phase-space trajectories for the different regimes in two-dimensional collisions, in the plane $\lambda = 2\pi/|\mathbf{k}| - \eta_x$, for different initial conditions: 1 – $\theta_0 = 8/4\pi$; $\lambda_0 = 10$ μm, 2 – $\theta_0 = 8/9\pi$; $\lambda_0 = 7$ μm, 3 – $\theta_0 = \pi/6$; $\lambda_1 = 5$ μm, 4 – $\theta_0 = 8/9\pi$; $\lambda_0 = 2$ μm, 5 – $\theta_0 = \pi/36$; and $\lambda_0 = 434.2$ nm, for an infinite width ionization front, with a 80 fs rise time, maximum electron density $n_{e0} = 5 \times 10^{20}$ cm^{-3}, and $\beta_f = 0.941$.

To illustrate the different regimes for the infinite width ionization front we have performed ray-tracing simulations, solving the equations of motion for the photons, Eqs. (1) and (2), with a fourth-order Runge-Kutta method. In this scenario, the ray-tracing simulations confirm the analytical results. First, it is instructive to examine the different photon phase-space trajectories, as shown in Fig. 1. The selected plasma and probe photon parameters that illustrate these regimes are currently obtainable in laboratory conditions [12,14,15]. Depending on the initial conditions, we observe that the photons are either reflected in phase space (trajectories 1 and 3), or transmitted in phase space (trajectories 2,4, and 5). More important, and unlike the one-dimensional scenario, even in the co-propagation scenario (where $\theta_0 \leqslant \pi/2$) we can observe reflection in phase space and a significant frequency upshift (trajectory 3), that cannot be attained for standard injection conditions in one-dimensional collisions. This is the most interesting scenario, since the co-propagating photons are injected in vacuum at some angle to the front, and then are overtaken by the front and reflected by the front again in the copropagation direction. This scenario maximizes the interaction time with the ionization front in the copropagation scenario, and it gives the highest frequency upshift when the conditions for reflection in the counterpropagation scenario (leading to a double Doppler upshift) are not met, as it usually happens for the standard experimental conditions. It is therefore the most interesting scenario to examine in detail.

In Fig. 2, we evaluate the frequency upshift for co-propagation scenarios as a function of the different free pa-

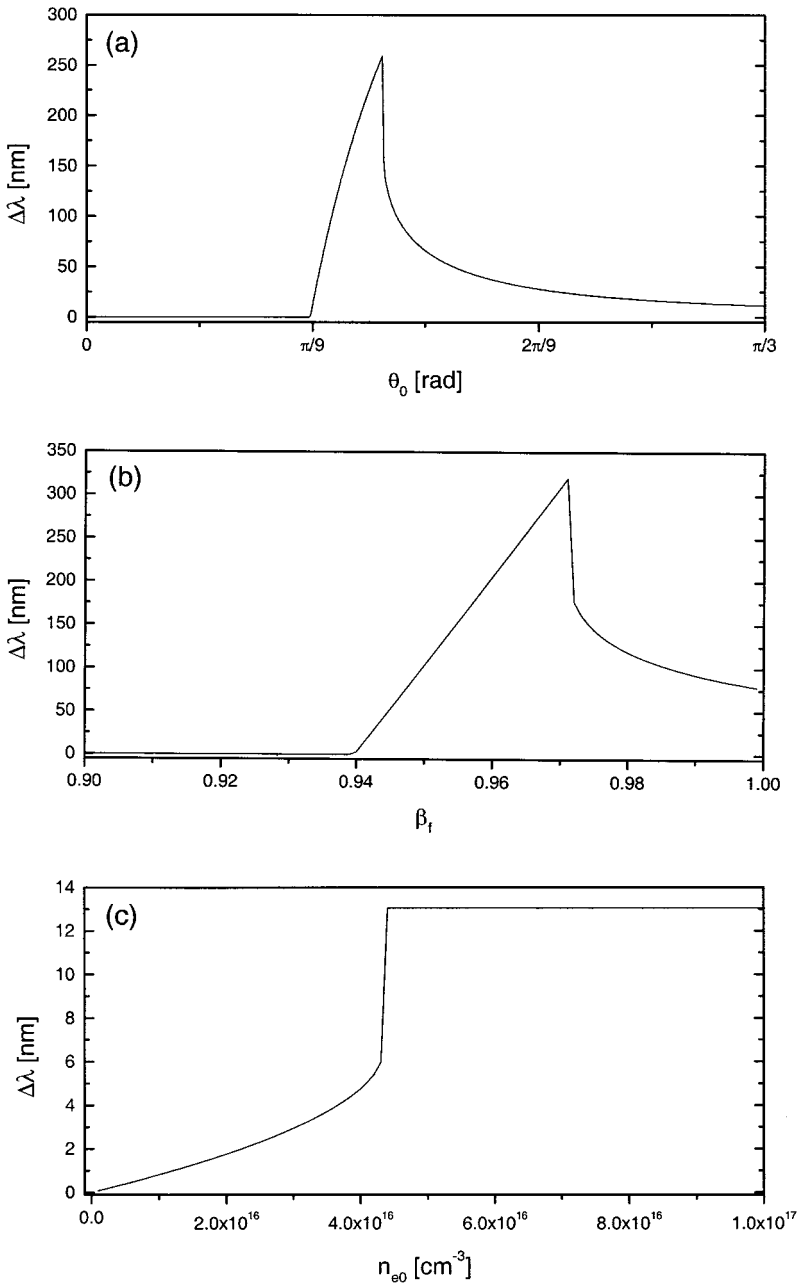

FIG. 2. Frequency upshift as a function of (a) θ_0, photon incidence angle (here, the asymptotic value for $\theta_0 \to \pi$ is 7.57 nm); (b) β_f, ionization front velocity; and (c) n_{e0}, ionization front density, keeping the remaining parameters constant, for $n_{e0}=5\times10^{19}$ cm^{-3}, $\beta_f=0.941$, and $\theta_0=\pi/9$.

rameters, by employing the analytical expressions derived before Eqs. (10) and (11), keeping the incident frequency of the probe photons constant. The remaining parameters that are kept constant are the ones available in the photon acceleration experiments by Dias and co-workers [12,14]. We immediately observe that a clear maximum exists for the highest frequency upshift in copropagation, and that by carefully tuning the ionization front parameters it is possible to observe frequency upshifts in excess of 200 nm $=\lambda_0/3$ [in Figs. 2(a) and 2(b)]. Furthermore, as can be seen in Fig. 2(c), the regime for reflection in co-propagation can be easily achieved with modest ionization front densities. These results indicate that even when the conditions for reflection in counterpropagation are not met, the frequency upshift in copropagation can be optimized, and tuned, over a wide range of frequencies, with frequency upshifts of the same order as the frequency of the incident photons.

Of course, only when the spot size of the probe laser pulse is much smaller than the width of the ionization front (or equivalently, the spot size of the ionizing laser), it is possible to talk about infinite ionization fronts [15]. In fact, in standard experimental conditions [10,12], the spot sizes are similar; therefore, it is almost mandatory to examine the features introduced by a finite width ionization front.

For finite width ionization fronts, the extra free parameter introduces new phenomenology. In fact, if we define our finite width ionization front as

$$\omega_{pe}^2(x-\beta_f ct)=\frac{\omega_{pe0}^2}{2}e^{-2y^2/W_0^2}\left\{1+\tanh\left(\frac{x-\beta_f ct}{c\tau_f}\right)\right\}, \tag{13}$$

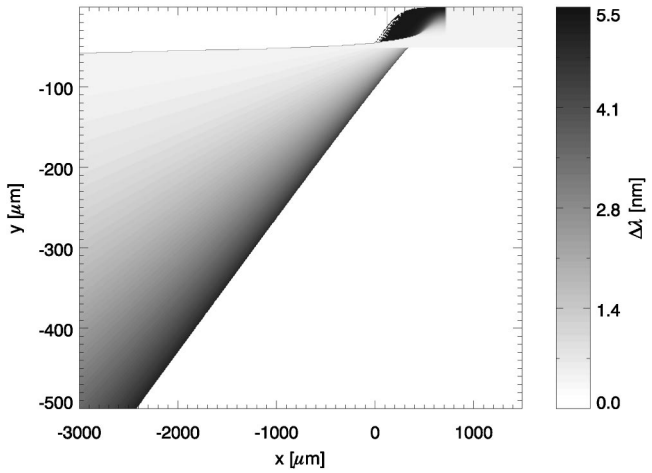

FIG. 3. Frequency upshift map for the collision of a slab of probe photons with $W_1=25\ \mu$m and $\lambda_0=800$ nm, colliding at an angle $\theta_0=\pi$, with an ionization front with $n_{e0}=5\times10^{19}\ \mathrm{cm}^{-3}$, $\beta_f=0.941$, $W_0=25\ \mu$m, and $\tau_f=80$ fs.

where y describes the transverse position, it is obvious that depending on the *collision point*, the probe photons will be impinging on the front at different angles. It is then expected that the frequency upshift will vary along the width of the probe photon beam, much in the same way as shown in Fig. 2(a). This is illustrated in Figs. 3 and 4, where we have solved the equations of motion for a photon beam with finite width colliding with a finite width ionization front, as described by Eq. (13) and where we have deposited on a grid in the xy plane of the collision (and for each time step) the local frequency of the photons, thus mapping the frequency of the photons along their propagation.

In Fig. 3, the standard scenario of transmission in counterpropagation is presented. As expected, the photons colliding, at $x=0$, head on with the center of the front (at $y=0$) suffer a stronger upshift, and also a stronger diffraction, while the photons colliding with the outer parts of the ionization front (at $y\approx2W_0\approx50\ \mu$m) remain almost unshifted.

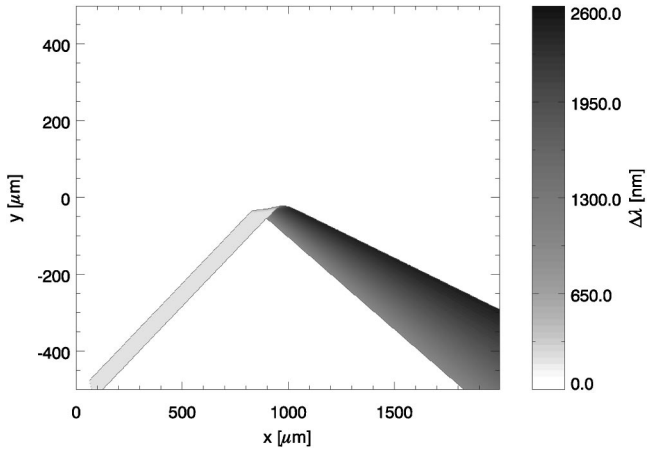

FIG. 4. Frequency upshift map for the collision of a slab of probe photons with $W_1=25\ \mu$m and $\lambda_0=5\ \mu$m, colliding at an angle $\theta_0=\pi/6$, with an ionization front with $n_{e0}=5\times10^{20}\ \mathrm{cm}^{-3}$, $\beta_f=0.941$, $W_0=25\ \mu$m, and $\tau_f=80$ fs.

From the photon trajectories long after being detached from the ionization front (at $x=-3000\ \mu$m), it is also clear that the ionization front is acting not only as a relativistic mirror but also as a diffraction grating, angularly spreading the photon beam with a well-defined frequency dependence. In Fig. 4, the photons are reflected in copropagation, and the frequency upshifts are stronger, and again the ionization front upshifts the photons, increases the bandwidth of the incident beam, and higher frequencies diffract at lower angles: the frequency upshifts, however, are lower than those predicted by the infinite ionization front results. This is due to the fact that the photons slip out from the ionization front density gradient region in a time smaller than the interaction time for an infinite width ionization front. In fact, if we analyze the frequency upshift in the same way as in Fig. 2, and for the same conditions of Fig. 2, but now for a finite width ionization front, we immediately observe lower upshifts by a factor of 5 at the maximum when varying θ_0 (Fig. 5), and this upshift is less sensitive to the front velocity [Fig. 5(b)], and essentially dependent on the maximum electron density of the ionization front for all collision angles; this is due to the fact that for a finite width ionization front the interaction time is strongly limited by the geometry of the front, and no longer by the front velocity, since the photons exit the index of refraction gradient sideways, before interacting completely with it, as occurs in the infinite width scenario.

Another peculiar aspect of finite width ionization fronts is that another regime can be achieved, when the probe photons enter the plasma behind the front. Now it is necessary to consider that the photons are injected in the plasma, overtake the ionization front, and then either propagate in vacuum or in the plasma, behind the ionization front. For this scenario to occur the photon group velocity in the plasma projected along the direction of the ionization front velocity, has to be greater than the ionization front group velocity, i.e.,

$$\mathbf{k}c/\omega\cdot\mathbf{e}_x>\beta_f\,. \tag{14}$$

For probe photons colliding with ionization fronts created by a similar laser pulse with a similar wavelength, the velocity of the front is similar to the velocity of the photons behind the plasma, which means that condition (14) is not easily satisfied. Therefore, this scenario does not seem to be relevant for the standard experimental conditions for the collision of probe photons with relativistic ionization fronts.

In summary, we have analyzed the two-dimensional collision of probe photons with relativistic ionization fronts employing ray-tracing theory and simulations. Besides pointing out the existence of a new regime that allows for strong frequency upshifts even in copropagation, we have demonstrated that finite width ionization fronts lead to smaller frequency upshifts than the infinite width fronts, but have the advantage of also acting as high-efficiency diffraction gratings, providing a well-defined angular spectral dispersion. Taming the relevant parameters where both of these scenarios can be tested and applied in laboratory conditions is the next step of this work.

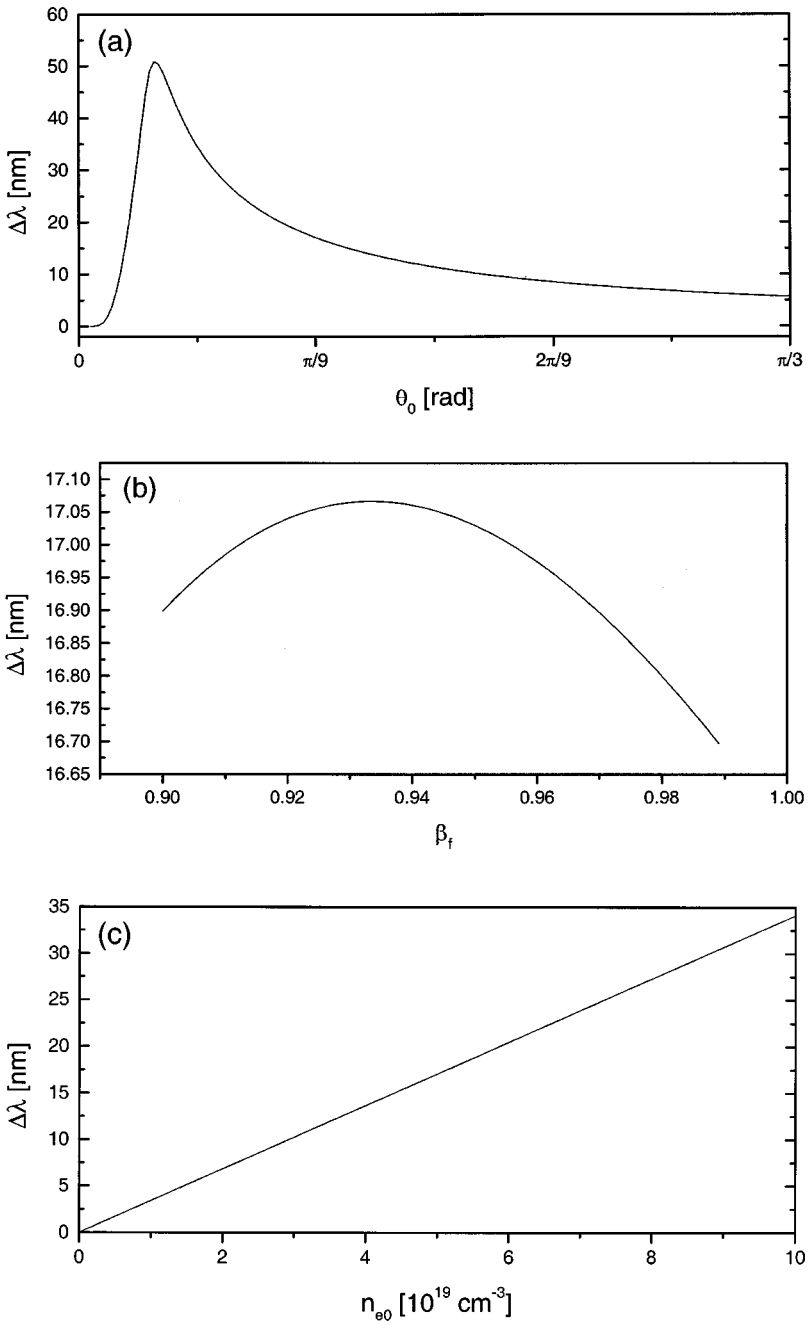

FIG. 5. Frequency upshift as a function of (a) θ_0, photon incidence angle (here, the asymptotic value for $\theta_0 \rightarrow \pi$ is 2.57 nm); (b) β_f, ionization front velocity; and (c) n_{e0}, ionization front density, keeping the remaining parameters constant, for a finite width ionization front with $n_{e0}=5 \times 10^{19}$ cm^{-3}, $\beta_f=0.941$, $\theta_0=\pi/9$, and $W_0 \approx 21$ μm.

This work was partially supported by FCT (Portugal), under Grant Nos. Praxis XXI/BPD/11804/97 and Praxis XXI/BD/3813/94.

[1] V. I. Semenova, Sov. J. Radiophys. Quantum Electron. **10**, 599 (1967).
[2] M. Lampe, E. Ott, and J. H. Walker, Phys. Fluids **10**, 42 (1978).
[3] J. T. Mendonça, J. Plasma Phys. **22**, 15 (1979).
[4] W. B. Mori, Phys. Rev. A **44**, 5118 (1991).
[5] R. L. Savage, Jr., C. Joshi, and W. B. Mori, Phys. Rev. Lett. **68**, 946 (1992).
[6] N. S. Stepanov, Sov. Phys. JETP **26**, 1234 (1968).
[7] J. T. Mendonça and L. O. Silva, Phys. Rev. E **49**, 3520 (1994).
[8] L. O. Silva and J. T. Mendonça, IEEE Trans. Plasma Sci. **24**, 316 (1996).
[9] J. M. Dias, L. O. Silva, and J. T. Mendonça, Phys. Rev. ST Accel. Beams **1**, 031 301 (1998).
[10] W. M. Wood, C. W. Siders, and M. C. Downer, Phys. Rev. Lett. **67**, 3523 (1991).

[11] W. M. Wood, C. W. Siders, and M. C. Downer, IEEE Trans. Plasma Sci. **21**, 20 (1993).
[12] J. M. Dias *et al.*, Phys. Rev. Lett. **78**, 4773 (1997).
[13] S. Weinberg, Phys. Rev. **126**, 1899 (1962).
[14] J. M. Dias *et al.* (unpublished).
[15] For further experimental results exploring these limits, see N. C. Lopes *et al.* (unpublished).